Inhibition of lens epithelial cell growth *via* immobilisation of hyaluronic acid on atmospheric pressure plasma modified polystyrene

Raechelle A. D'Sa,*[a] Peter J. Dickinson,[a] Jog Raj,[a] Barbara K. Pierscionek[b] and Brian J. Meenan[a]

Received 7th September 2010, Accepted 25th October 2010
DOI: 10.1039/c0sm00936a

Naturally occurring macromolecules have the potential for providing non-fouling coatings on substrates based on a steric entropic principle. In order for this effect to occur, the macromolecules that adhered to the surface must have the correct chemical conformation. This article reports on the immobilisation of hyaluronic acid (HA) onto polystyrene substrates for the purpose of repelling cellular adhesion thereon. In order to create a polystyrene surface capable of adhering HA in the required orientation substrates were treated by atmospheric pressure plasma processing in air. The resulting oxidised surfaces were then aminated by the chemisorption of the 3-aminopropyltrimethoxysilane (APTMS) linker molecule. Three distinct chemical states were found for the APTMS amine group: a neutral, a protonated and a hydrogen bonded state, as determined by X-ray photoelectron spectroscopy (XPS). Carbodiimide coupling of HA at two different macromolecular concentrations (1 mg cm^{-3} and 3 mg cm^{-3}) to the aminated surfaces on oxidized polystyrene resulted in covalent immobilisation of the polysaccharide. The chemistry and topography of the polymer surface at each stage of the coating process were analysed by a combination of XPS, ToF-SIMS, and AFM. XPS demonstrates that HA was successfully grafted to the aminated PS surfaces. The degree of chemical homogeneity on the surfaces was determined by ToF-SIMS. Changes in topography resulting from the immobilization process were evident in the AFM images. *In vitro* studies of the response of human lens epithelial cells (LEC) to the HA-modified polystyrene indicated a significant reduction in cell numbers at all time points post-seeding compared to the control. These results coupled with the surface analysis data indicate that the immobilization method based on atmospheric plasma activation of the polymer surface creates a HA layer with a steric conformation capable of inhibiting cellular attachment.

1 Introduction

The success or otherwise of medical implants and thereby the biomaterials from which they are fabricated is crucially reliant on the nature of protein and cellular response at their surfaces.[1,2] In many cases, fouling of implants from adverse biological interactions can result in severe clinical complications such as coagulation, complement activation, thrombus formation, fibrous encapsulation, and immunological reactions.[3,4] Interfacial forces between a biomaterial and proteins are known to have implications on the nature of any subsequent cellular response.[5,6] These forces are modulated by the chemistry of the biomaterial and include electrostatic interactions, hydration effects, dispersion forces and steric–entropic effects. It is generally accepted that a "non-fouling" biomaterial interface can be created by grafting highly hydrated hydrophilic polymeric macromolecules onto its surface. This type of surface modification is important for various applications ranging from medical diagnostics and therapeutics to water purification.[6] However, for this strategy to be effective it has been recognised that the chemical conformation of the grafted adlayer must provide for the correct steric effects leading to an excluded volume condition, *i.e.* repulsion of proteins by trapped water in a "brush-like" macromolecular surface structure.[7] One of the most common hydrophilic polymers employed for this purpose is poly(ethylene glycol) (PEG), which when immobilised onto biomaterial surfaces in the requisite conformation confers protein and cell resistance.[7–12] However, PEG is known to be oxidised in an *in vivo* environment, making functionalisation with alternative polymers attractive. Naturally occurring macromolecules such as polysaccharides are a promising alternative to PEG for providing non-fouling coatings for biomedical purposes. Such polysaccharides have extensively hydrated hydrogel-like, mobile molecular chains, that if immobilised with the appropriate architecture can act as a steric–entropic barrier in a similar manner to PEG.

Hyaluronic acid (HA) is an example of a polymer that can be employed for this purpose.[13–16] HA belongs to the glycosaminoglycan (GAG) family, however unlike other GAGs it is not sulfated and does not therefore bind covalently to any proteins. It is present ubiquitously in the extracellular matrix, vitreous humour, synovial fluid and cartilage.[17,18] It is a linear polymer of high molecular weight comprising a glucuronic acid (1-β-3) *N*-acetylglucosamine (1-β-4) disaccharide repeating unit. In solution, HA takes on the form of an expanded, highly hydrated coil structure with a radius of gyration of approximately 200 nm and in its hydrated state has a1000-fold more water than polymer.[19] It plays an important role in the hydrodynamic properties of the extracellular environment and provides structural support for other matrix components.[20] It is used clinically in ophthalmics to

[a]*Nanotechnology and Integrated Bio-Engineering Centre (NIBEC), University of Ulster, Shore Road, Newtownabbey, Co. Antrim, BT37 0QB, Northern Ireland, UK. E-mail: r.dsa@ulster.ac.uk; raechelledsa@gmail.com; Tel: +44 (0)2890368663*
[b]*Vision Science Research Group, School of Biomedical Sciences, University of Ulster, Coleraine, Co. Londonderry, BT52 1SA, UK*

accelerate corneal wound healing in ocular surgeries.[21] Its ability to promote water retention is thought to be the cause of tear fluid stability in the eye and therefore HA is used extensively in eye drop solutions.[22,23] It is also used as a viscoelastic fluid in intraocular surgeries to relieve intraocular pressure.[24]

A number of procedures have been employed for the immobilisation of HA onto biomaterial surfaces ranging from physisorption to chemisorption techniques.[14,16,25–30] However, many of these approaches require relatively complicated synthetic protocols to ensure the presence of specific surface functional groups. Thus, there still exists an ongoing need for versatile immobilisation strategies that are capable of robustly and covalently tethering HA onto a variety of medically relevant biomaterials, particularly inherently hydrophobic polymers. Modification of polymer surfaces to create a so-called "bonding layer" which can then be utilised for the immobilisation of macromolecules such as HA has been employed effectively.[31,32] Whereas plasma processing has been used in this regard, it is not widely applied due to the high engineering costs associated with vacuum based plasmas that are normally required to carry out these reactions.[26,33,34] Hence, atmospheric pressure plasma processing offers an attractive alternative since it allows for rapid, continuous in-line processing and lower operational costs. The facility offered by normal "corona" based methods is limited in this regard due to the transient nature of the surface effects induced. However, the advent of dielectric barrier discharge (DBD) atmospheric pressure processing holds out more promise, but its ability has yet to be fully realised.[35–38]

This article reports a study of the use of DBD processing to create an oxidised "bonding layer" on polystyrene (PS) substrates to support the subsequent immobilisation of HA. The role of this substrate functionalisation is to enhance and direct the subsequent chemisorption of the widely used 3-aminopropyltrimethoxysilane (APTMS) group. Carbodiimide linker chemistry is then used to graft the carboxylic acid groups in HA onto the APTMS layer. Each of the separate stages of the immobilisation treatment using 1 mg cm^{-3} and 3 mg cm^{-3} HA solutions is followed by X-ray photoelectron spectroscopy (XPS) and time of flight secondary ion mass spectrometry (ToF-SIMS) analysis. Atomic force microscopy (AFM) is employed to further elucidate the changes imparted by the processing steps. The response of human lens epithelial cells (LECs) to covalently immobilised HA was determined via *in vitro* adhesion and proliferation studies. These data along with those from the various surface analyses have been used to evaluate the nature of the chemical conformation of the HA coating in the context of the steric requirements known to cause inhibition of cell adhesion. PS has been used in this study as a model polymer to investigate the efficiency of grafting as it is the gold standard for tissue engineering applications. Grafting of HA onto more ophthalmic relevant polymers such as acrylics and silicon elastomers is currently underway and will be reported elsewhere.

2. Materials and methods

2.1 Materials

Commercial grade polystyrene (PS), as 1.2 mm thick sheets (Goodfellow, Cambridge UK), was used as the polymer substrate for these studies. The sheets were cut into 1.5 × 1.5 cm^2 sized squares for chemical and topographical analysis. Discs of 34 mm diameter were punched from the polymer sheets for use in all the cell culture studies and associated assays with the exception of the immunofluorescence staining studies which used 22 mm diameter discs. Samples were cleaned by sonication in ethanol for 15 min and dried in air overnight prior to use. Hyaluronic acid (HA), as the sodium salt from the *Streptococcus equi* species (Fluka, UK), was used as received. Water-soluble 1-ethyl-3(3-dimethylaminopropyl)carbodiimide hydrochloride (EDC, Fluka, UK), *N*-hydroxysuccinimide (NHS, Sigma-Aldrich), (3-aminopropyl)trimethoxysilane (APTMS, Sigma-Aldrich, UK), and 2-(*N*-morpholino)ethanesulfonic acid (MES) were all used as received.

2.2 Atmospheric pressure plasma treatment of polystyrene

Surface modification of PS was carried out at atmospheric pressure using a dielectric barrier discharge (DBD) system (Arcojet Gmbh, Germany). The operational characteristics of the DBD reactor (Arcotec GmbH, Germany) have been described in detail elsewhere.[28–30] In brief, samples were placed on the moving ground electrode and treated at varying energy doses (D) corresponding to a range of different power densities (P_d) and residence times in the plasma (R) delivered *via* three working electrodes adjacent to the platen. All experiments were carried out at a platen transit speed through the plasma region of 0.48 m s^{-1}. An explanation of the known effects of the various experimental conditions used in DBD has been reported elsewhere.[39–42]

2.3 Immobilisation of hyaluronic acid onto DBD treated polystyrene

HA was immobilised onto the DBD modified PS by silanisation and subsequent grafting by the carbodiimide mediated coupling *via* the reaction pathways illustrated in Scheme 1.

DBD treated PS samples were immersed in a 10% w/w solution of (3-aminopropyl)trimethoxysilane (APTMS) in methanol for 60 s to silanise the surface. The silanised samples were washed with methanol and dried in an oven at 50 °C for 2 h. HA was dissolved in a solution of 0.01 M MES buffer at concentrations of (a) 1 mg cm^{-3} and (b) 3 mg cm^{-3}. The carboxylic acid group of the HA molecule was activated by adding NHS and EDC sequentially to make up a solution with final concentrations of 0.05 M NHS and 0.2 M EDC. This activated HA solution was stirred for 1 h at room temperature prior to immersion of the silanised polymer samples and incubation at room temperature overnight on a rocker table. Samples were then washed with Milli-Q ultrapure water for 24 h, dried at room temperature and pressure and stored in sterile Petri dishes prior to analysis.

2.4 Surface analysis

2.4.1 XPS analysis. X-Ray photoelectron spectroscopy (XPS) was carried out using a Kratos Axis Ultra DLD spectrometer (Kratos, UK) at a base pressure of $<5 \times 10^{-8}$ Torr. A monochromated AlKa X-ray (1486.6 eV) source operating at an anode voltage of 15 kV and a 10 mA current was employed. A "slot" aperture was used to limit the area of analysis to 700 μm ×

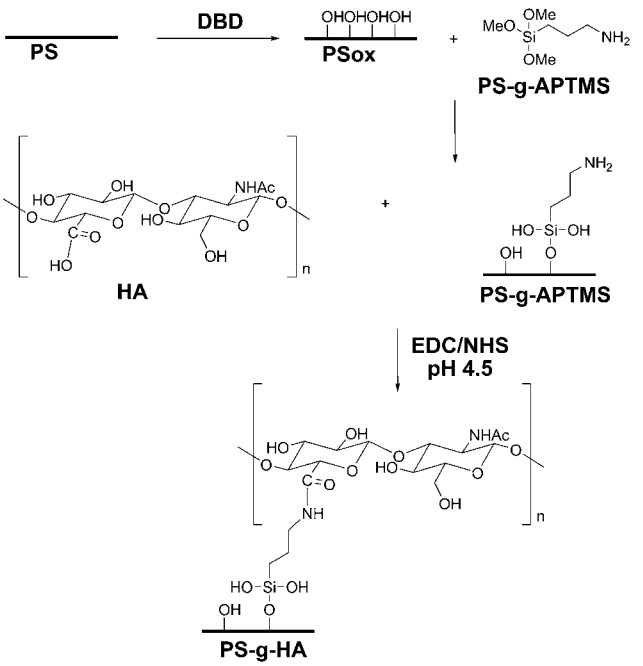

Scheme 1 Immobilisation of HA onto PMMA surfaces.

300 μm. Wide energy survey scans (1–1300 eV) were recorded at pass energy 160 eV and high resolution spectra at 20 eV. A magnetic immersion lens was used as the primary means to neutralise the effects of residual electrical charge generated on the insulating polymer surfaces. Binding energy (BE) positions were further corrected for charging effects by setting the lowest C 1s component to 285.0 eV.[43] Quantitative analysis of three separate areas on each sample was achieved using CasaXPS version 2.3.12 software (Casa Software, UK) by subtraction of a linear background and determination of areas for the most intense spectral lines for all the elements detected. Data are reported as average values of relative atomic % concentration (at.%) ± 1 standard deviation. Spectra were curve fitted (after background subtraction) using a mixed Gaussian–Lorentzian (70 : 30) function using established peak positions. The electron attenuation length of the C 1s photoelectron in a polymeric matrix can be assumed to be ~3 nm.[44] This corresponds to an approximate value for the sampling depth of 10 nm when the emission angle is normal to the surface.[45] Therefore 95% of the detected signal originates from this sampling region.

2.4.2 ToF-SIMS analysis. Time-of-flight secondary ion mass spectrometry (ToF-SIMS) measurements were performed using a ToF-SIMS V (ION-TOF GmbH, Germany) instrument. A bismuth liquid metal ion gun (LMIG) generating Bi_3^{++} cluster ions was used as the primary ion source operating with the reflectron analyser and microchannel plate detector with post-acceleration of 20 kV. The primary ion dose for all analyses was kept within static SIMS limit (*i.e.* $<10^{12}$ cm^{-2}). Spectral acquisition and image analyses were carried out using IonSpec Version 4.1.0.1 and IonImage Version 3.1.0.14 software, respectively (ION-TOF GmbH, Germany). Pulses of low energy electrons from a flood gun were applied to samples between periods of secondary ion collection to compensate for charging effects. Positive ion spectra from the various surfaces were recorded as *m/z versus* intensity plots and key ions identified for subsequent imaging studies. Mass resolved secondary ion images for selected ions were recorded with the Bi_3^{++} cluster ion source in burst alignment mode. Three replicate false-colour images in positive ion collection mode were recorded for each sample type.

2.4.3 AFM analysis. AFM was used to compare the topographical features created after DBD surface modification and subsequent stages of HA chemical immobilisation. A Digital Instruments (DI) NanoScope SPM (Vecco Metrology Group, USA) operating in tapping mode under ambient conditions was used. Images were acquired with a silicon tip mounted on a cantilever with a spring constant of 40 N m^{-1} operating at a resonant frequency of 300 kHz and scan rate 1 Hz. Samples were analysed over a 1.0 μm × 1.0 μm sample area at a resolution of 512 × 512 pixels and false-colour images produced using NanoScope 6.11r1 software (Vecco Metrology Group, USA). Zero-order plane fitting was used to remove the image bow that can result from the scanner moving out of plane with the sample. Possible errors in piezo linearities were corrected for by zero and first order flattening. Both the mean surface roughness (R_a) and root mean square roughness (R_q) values were calculated from imaging of three replicates of each sample type.

2.5 Biological analysis

2.5.1 Cell culture. Samples for *in vitro* cell studies were sterilised by placing them in 70% aqueous ethanol for an hour and leaving them to dry in a laminar flow hood. Agar was used as a gelling agent to stick the polymeric substrates to the six-well plates in order to avoid cells adhering to the under side of the substrates. A stock solution of 0.6% Agar (Sigma-Aldrich, UK) in Milli-Q water was freshly prepared and autoclaved at 123 °C for 15 min. Molten Agar (200 μm) was pipetted into sterile six-well plates followed by careful placement of the polymer samples.

Immortalised human LECs (CRL-11421) were used to assess cell response to immobilized HA on DBD processed PS surfaces. Cells were grown in a humidified atmosphere of 5% CO_2 in Dulbecco's minimum essential medium (DMEM, Gibco, UK) that was supplemented with 20% foetal bovine serum (FBS, Sigma, UK), 100 IU mL^{-1} penicillin G, 100 mg mL^{-1} streptomycin sulfate, and 20 mg mL^{-1} gentamycin (all obtained from Invitrogen, UK). The cells were maintained at below 70% confluency and were passaged every three to four days using 0.05% trypsin–EDTA (Sigma, UK). The cells were seeded on the variously processed PS polymer discs at a concentration of 2 × 10^5 cells per cm^2 and cultured under normal humidified conditions at 37 °C, 5% CO_2 for 4, 24 and 48 h, respectively. Cell media was changed every 2 days.

2.5.2 Crystal violet adhesion assay. LECs were seeded onto the polymer samples placed in the Agar pre-coated six-well plates and incubated for 4 h at 37 °C in a humidified 5% CO_2 atmosphere. The media was aspirated off and the cells were washed twice with PBS (Gibco, UK) and the adhered cells were morphologically fixed using a 10% paraformaldehyde (PFA, Sigma-Aldrich, UK) solution. After 15 min the samples were washed with PBS followed by a 1 : 4 methanol : PBS solution for further 15 min. The cells were then stained with a 0.5% crystal

violet in 1 : 4 methanol : PBS solution for 30 min. The samples were again washed with PBS and the stained cells solubilised by adding 800 μL of a 10% glacial acetic acid solution (Sigma-Aldrich, UK) to each well and placing the well plates on a gyro-rocker for 30min. Aliquots (200 μL) of the solution from each sample type was transferred in triplicate to a 96-well plate, giving a total of 9 replicates per sample type. The absorbance (optical density) of the solutions was read in a Tecan Sunrise™ (TECAN Austria GmbH) microplate reader (equipped with Magellan Software) using a 570 nm filter.

2.5.3 MTT cell viability assay. A stock solution of 5 mg cm^{-3} [3-(4,5-dimethylthiazol-2-yl)-2,5-diphenyltetrazolium bromide] (MTT, Sigma-Aldrich, UK) in PBS was prepared and passed through a 0.2 mm filter before storage at 4 °C. LECs were cultured on each substrate type according to the method outlined above. After 24 h and 48 h post-seeding, the culture media was replaced with 2 cm^3 of phenol-free DMEM media (Gibco, UK) containing the MTT solution at a concentration of 500 μg cm^{-3}. The cells were then placed in the incubator at 37 °C and 5% CO_2 until the formazan product was visible (~1.45 h). The culture medium was aspirated off and the cells were solubilised by adding 350 μL of 0.1 M HCl in propanol to each well and placing the plates on a gyro-rocker aliquots for 10 min. A 100 μL aliquot of the solution from each well was transferred in triplicate to a 96-well plate, giving a total of 9 replicates per sample type. The absorbance (optical density) for each solution was read in a Tecan Sunrise™ (TECAN GmbH, Austria) microplate reader using a 570 nm filter.

2.5.4 Immunocytochemistry. Cells were cultured for 24 h on the various substrates as before. Samples were washed with PBS at 37 °C and permeabilised using 4% PFA with 0.1% Triton X-100 in PBS for 20 min. The samples were washed with PBS to remove any traces of PFA. To visualize cytoskeletal actin, samples were incubated with phalloidin Alexa Fluor 488 (Molecular Probes, UK) at a concentration 25 U cm^{-3}. The samples were rinsed three times in PBS and mounted with Vectashield Mounting Medium containing 1.5 μg cm^{-3} of 4′-6-diamidino-2-phenylindole (DAPI) counterstain (Vector Laboratories, UK). Cells were examined using an epifluorescence microscope (Nikon Eclipse 80*i*).

2.5.6 Statistical analysis. All assays were carried out in triplicate and repeated three times to confirm results. Results are reported as mean ± standard deviation. Statistical analysis of all the surface analysis data and that from the biological assays was performed with Origin® (v. 7.0383, OriginLab Corporation, USA). One way analysis of variance (ANOVA) was used to compare mean values to determine equivalence of variance between pairs of samples. Significance between groups was determined using the Bonferroni multiple comparison test. A value of $p < 0.05$ was taken as statistically significant.

3 Results and discussion

3.1 Surface grafting with HA

3.1.1 X-Ray photoelectron spectroscopy (XPS). The HA grafted surfaces were prepared by the three step modification process shown in Scheme 1. In the first step, the DBD plasma treatment technique generates reactive species that are transferred to the polymer surface through a flux of neutral particles, electrons, ions and radicals, as well as from exposure to UV radiation. These high energy species bombard the substrate such that it undergoes a variety of chemical and physical process leading to surface modification of the PS mainly through radical initiated reactions. The radicals generated include carbon radicals, oxygen radicals and peroxy radicals which can further react with oxygen or moisture in the ambient air to generate oxygen functionality on the surface such as hydroxyls and hydroperoxides. In the DBD process the energetic species generated are produced in discrete pulses, with durations in the tens of nanoseconds time scale. This so-called 'cold' plasma condition keeps surface damage by thermal effects to a minimum.

In the second step, these hydroxyl or hydroperoxide groups react with APTMS to generate an amino-functionalised surface. The third step then involves a carbodiimide mediated grafting of HA. The carboxylic acid groups of HA were activated by EDC/NHS at pH 4.5 for an hour before the anchoring of HA onto the APTMS linker took place. As indicated, in this work two different concentrations of HA were used in order to determine the lowest concentration of HA required for efficient grafting.

XPS was used to confirm the success of each step of the process as indicated by the respective wide energy survey scans (WESS) shown in Fig. 1a–e. Corresponding quantitative data for the pristine PS, DBD modified PS (PSox) and the HA grafted PS surfaces (PS-*g*-HA_{1mg} and PS-*g*-HA_{3mg}) are given in Table 1 and the results from deconvolution of the C 1s spectral region in each case are provided in Table 2. Pristine PS contains the expected aromatic and aliphatic C–C/C–H peaks centered at 285.0 eV and the characteristic π–π* (292.0 eV) shake up satellite contribution (Table 2). As pristine PS has no oxygen in its structure, oxidation of the surface by the DBD process can be accurately quantified post-treatment. Curve fitting of the corresponding C 1s envelope of PSox (Table 2) indicates new contributions to the polymer surface from components at *C*–O (286.5 eV), *C*=O (287.5 eV), O=*C*–O (289.0 eV).

Immediately after plasma treatment, the PSox surfaces were exposed to the APTMS linker molecule. The emergence of the Si 2p and N 1s peaks in the XPS data (Fig. 1c and Table 1) confirms the presence of the aminosilane linker molecule. Furthermore,

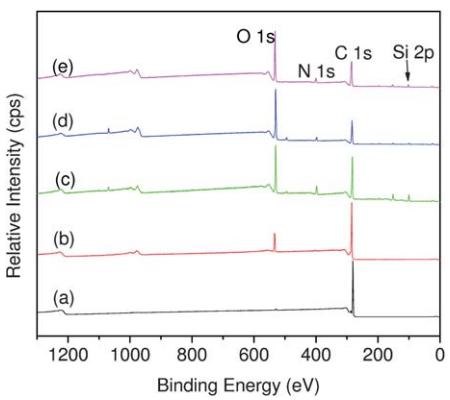

Fig. 1 Wide energy XPS survey scans for (a) pristine PS, (b) Psox, (c) PS-*g*-APTMS, (d) PS-*g*-HA_{1mg} and (e) PS-*g*-HA_{3mg} surfaces.

Table 1 XPS derived at.% values for each stage of the process leading to HA immobilisation on PS

	At.%			
	O 1s	N 1s	C 1s	Si 2p
PS	0	0	100	0
PSox	12.9 ± 1.9	0	82.2 ± 1.4	0
PS–APTMS	26.0 ± 0.0	9.9 ± 0.3	55.1 ± 0.6	9.0. ± 0.2
PS-*g*-HA_{1mg}	29.3 ± 0.2	10.2 ± 0.6	59.9 ± 0.6	0.7 ± 0.0
PS-*g*-HA_{3mg}	30.0 ± 0.2	9.7 ± 0.3	58.2 ± 2.0	2.0 ± 0.0
Theoretical APTMS	27.3	9.1	54.5	9.1
Theoretical HA	42.3	3.8	42.3	0

Table 2 XPS derived at.% for the contributions to the deconvoluted C 1s spectral envelope for each stage of the process leading to HA immobilisation on PS

	At.%		
	C–C/C–H	C–O/C–N	C=O/O=C–N
PS	100	0	0
PSox	63.0 ± 4.3	25.8 ± 1.9	11.2 ± 2.1
PS–APTMS	52.6 ± 1.7	38.0 ± 1.2	9.4 ± 1.1
PS-*g*-HA_{1mg}	28.7 ± 0.2	48.0 ± 0.1	23.1 ± 0.0
PS-*g*-HA_{3mg}	21.9 ± 0.9	56.9 ± 1.5	20.7 ± 0.1
Theoretical APTMS	40	60	0
Theoretical HA	7.1	64.3	28.6

the high resolution C 1s XPS data shows an increase in the C–O/C–N component at 286.3–286.5 eV which is indicative of the presence of the APTMS layer. The at.% concentration data for the experimentally acquired APTMS layer is very close to that of the expected theoretical values (Table 2). It is assumed that the small discrepancies in the values arise from a specific orientation of the molecule on the surface that reduces the number of methoxy groups and increases the silanol groups within the depth of analysis for the XPS technique. This orientation of the linker molecule can be deduced by curve fitting the N 1s peak as indicated in Fig. 2a. Previous studies have stated that between one and three chemical states of nitrogen are present for APTMS.[46–53] In this work, the nitrogen associated with the APTMS layer produced on the DBD modified PS surface, exists in three states: protonated, hydrogen-bonded and free amine related to components in the N 1s peak at 401.5, 400.4 and 399.3 eV, respectively (Fig. 2a).

Several authors have proposed mechanisms for the adsorption of APTMS which can explain the presence of the three states of nitrogen, as shown schematically in Fig. 3.[53–56] In this regard, the APTMS molecule can adopt any of the following chemical conformations: (a) APTMS covalently attached *via* a siloxane bond and terminated with a free amine, (b) the amino group of a free APTMS molecule hydrogen-bonded to the surface, (c) the APTMS molecule bent over to hydrogen-bond an amino group with an adjacent surface moiety and (d) the amino group on APTMS with an intra-molecular hydrogen bond to a silanol group. Based on the XPS results presented here, it would seem that all four of these conformations co-exist on the DBD treated PS surface.

As per the Scheme 1, the third step in overall process is the covalent attachment of HA to the amino functionalised surface by EDC/NHS to form an amide bond. In the associated XPS analysis, this leads to a decrease in the Si 2p contribution originating from the underlying APTMS layer upon HA immobilisation which falls from 9.0% to 0.7% (Fig. 1d and e and Table 1), thereby confirming that grafting occurs. Upon grafting, the C 1s spectral region changes considerably with an increase in polar functionalities corresponding to C–N/C–O at 286.3–286.5 eV and C=O and O=C–N at 288.0 eV observed. These results are in agreement with previously reported XPS data for HA.[25,26,30] The N 1s spectral region, as seen in Fig. 2b, indicates that the amount of protonated amine at 401.5 eV decreases with respect to the PS–APTMS surface. The corresponding presence of more amide functionality at 399.5 eV may be due to the formation of an amide bond between the carboxylate group on HA with the amino functionalised surface. As the Si 2p peak resulting from

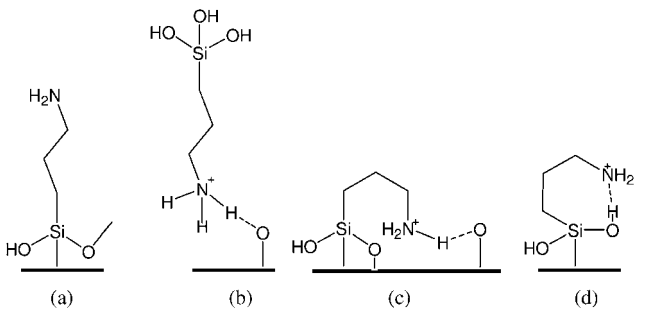

Fig. 3 Schematic illustration of APTMS adsorption mechanisms proposed by Kristensen *et al.* (ref. 53), Kowalczyk *et al.* (ref. 54), Horr and Arora (ref. 55), and Chiang *et al.* (ref. 56) The APTMS (a) molecule covalently attached *via* siloxane bond, (b) free molecule associates with the surface through H-bonding of the amino group, (c) molecule bends over to H-bond with adjacent surface moiety, and (d) molecule with intra-molecular bond to a silanol group.

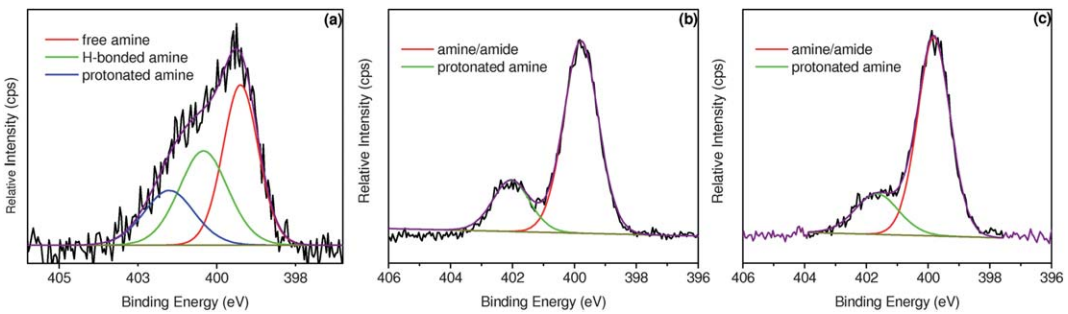

Fig. 2 Curve fitted N 1s XPS spectra for (a) PS–APTMS, (b) PS-*g*-HA_{1mg} and (b)PS-*g*-HA_{3mg}.

the APTMS does not disappear after HA grafting, this suggests that HA is not present as a complete monolayer and/or the grafted layer is thinner than the XPS sampling depth (~5 to 10 nm). This may be the cause of the discrepancy between the experimentally measured at.% concentration and the expected theoretical values. XPS analysis of both the HA grafted layers at both concentrations shows peaks that originated from the underlying APTMS layer indicating that in the "dry state" these coatings are thinner then the XPS sampling depth (~5 to 10 nm).

3.1.2 ToF-SIMS analysis. In order to further characterise the HA functionalisation of PS surfaces, ToF-SIMS imaging in the positive ion mode was used. The major advantage of ToF-SIMS is the ability to analyse only the outermost surface layer (2–3 nm) of a sample and provide not only information on the elemental composition but also the chemical structure of any species on the surface. Additionally, ToF-SIMS imaging can provide a valuable insight into the homogeneity of the surface condition after each of the steps involved indicating lateral uniformity on a scale of approximately 100 μm^2. The data obtained confirm that DBD induced oxidation of PS, followed by silanisation and subsequent coupling of HA with the surface bound chemical linker groups were all carried out successfully. The appearance of several major nitrogen mass fragments originating from the APTMS and HA layers at *m/z* 30, 41 and 58 amu corresponding to CH_4N^+, $C_2H_3N^+$ and $C_3H_8N^+$ respectively confirm the homogeneous grafting of these layers. In these analyses, PS is characterised by its most intense peak at *m/z* 91 amu which is due to the stabilised tropylium ion which is present in both the pristine and DBD modified polymer (Fig. 4a and b respectively). Fig. 4c shows a decrease in the intensity of the tropylium ion peak with the chemisorption of the APTMS layer. However, the presence of this species indicates that this layer is less than the ToF-SIMS sampling depth of 2–3 nm. After grafting of the HA layer onto the PS-*g*-APTMS surface, the intensity of the tropylium ion peak drops almost to zero, indicating that the combined APTMS-HA layer is approximately 2–3 nm thick. These data are in agreement with the XPS data which indicate that the HA layer is less than the sampling depth of this technique, *i.e.* ~5 to 10 nm.

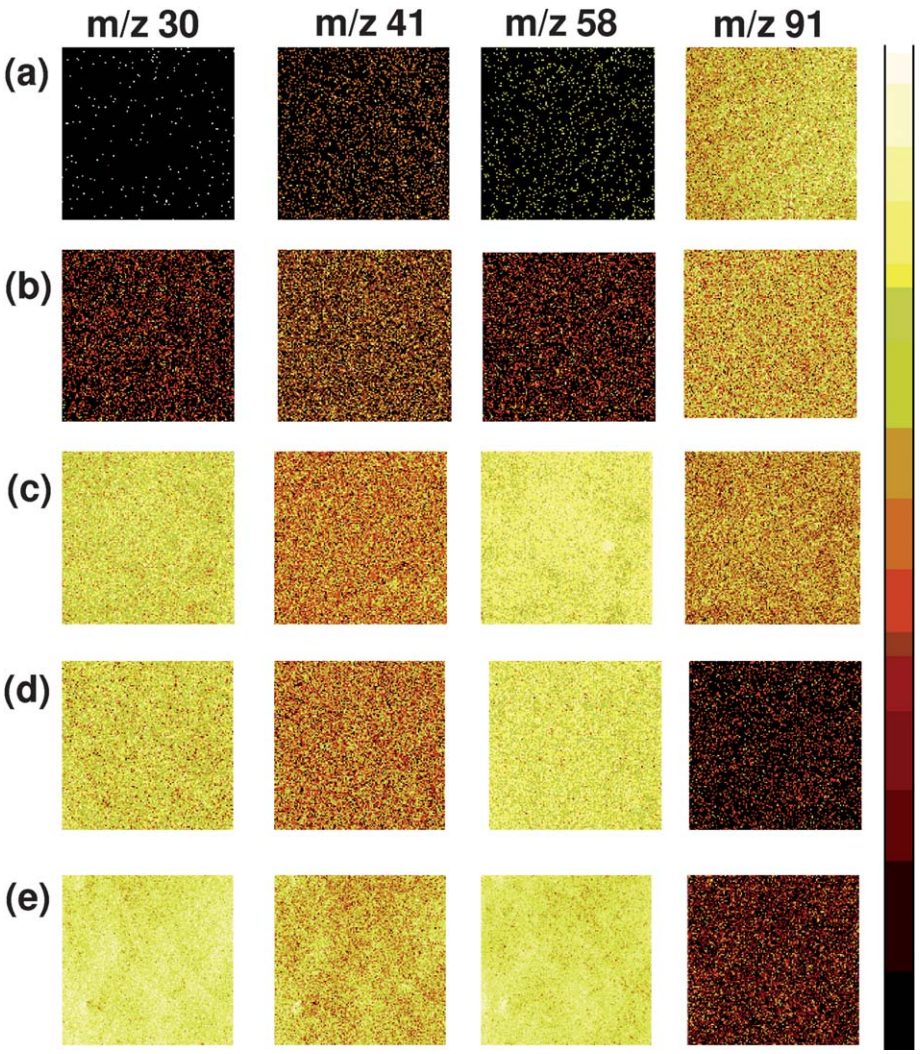

Fig. 4 ToF-SIMS images (100 μm × 100 μm) created from the positive ion counts detected at *m/z* 30, 41, 58, and 91 amu for (a) pristine PS, (b) Psox, (c) PS-*g*-APTMS, (d) PS-*g*-HA_{1mg} and (e) PS-*g*-HA_{3mg} (intensity scale shows increasing ion counts from dark to light coloured areas).

3.1.3 Atomic force microscopy (AFM). The morphology of pristine and the variously modified PS surfaces was measured by AFM. The resulting pseudo-3D images and surface roughness values are given in Fig. 5. The surface of pristine PS was relatively smooth with a roughness value (R_a) of 1.5 ± 0.2 nm. The DBD plasma treated polymer (PSox) showed a slight increase in roughness with a R_a value of 2.0 ± 0.1 nm. This indicates that the DBD treatment generates oxygen functionalities without causing significant etching of the polymer surface. The formation of the APTMS layer resulted in a slightly smoother surface (R_a = 1.6 ± 0.3 nm), possibly due to the fact that the chemisorbed APTMS layer masks some of the surface roughness. The PS–APTMS–HA_{1mg} surface had a R_a value of 1.7 ± 0.3 nm, which is again lower than the DBD treated surface and almost identical to that for the APTMS linker layer. These results tend to corroborate the interpretation of the ToF-SIMS images in that they confirm the homogeneous nature of the surfaces created in the grafting steps of the grafting procedure. The PS-*g*-HA_{3mg} surface, however, showed a significant increase in surface roughness to a R_a value of 4.1 ± 0.4 nm (R_a). It is assumed that this results from aggregation of the HA macromolecules present at this concentration.

3.2 Lens epithelial cell response

The initial attachment of LECs to pristine PS, DBD modified PS (PSox) and the HA grafted PS surfaces (PS-*g*-HA_{1mg} and PS-*g*-HA_{3mg}) was observed 4 h post-seeding. The same density of cells was seeded onto all surfaces. Optical micrographs of the cells adhered to each sample surface are presented in Fig. 6. The LECs

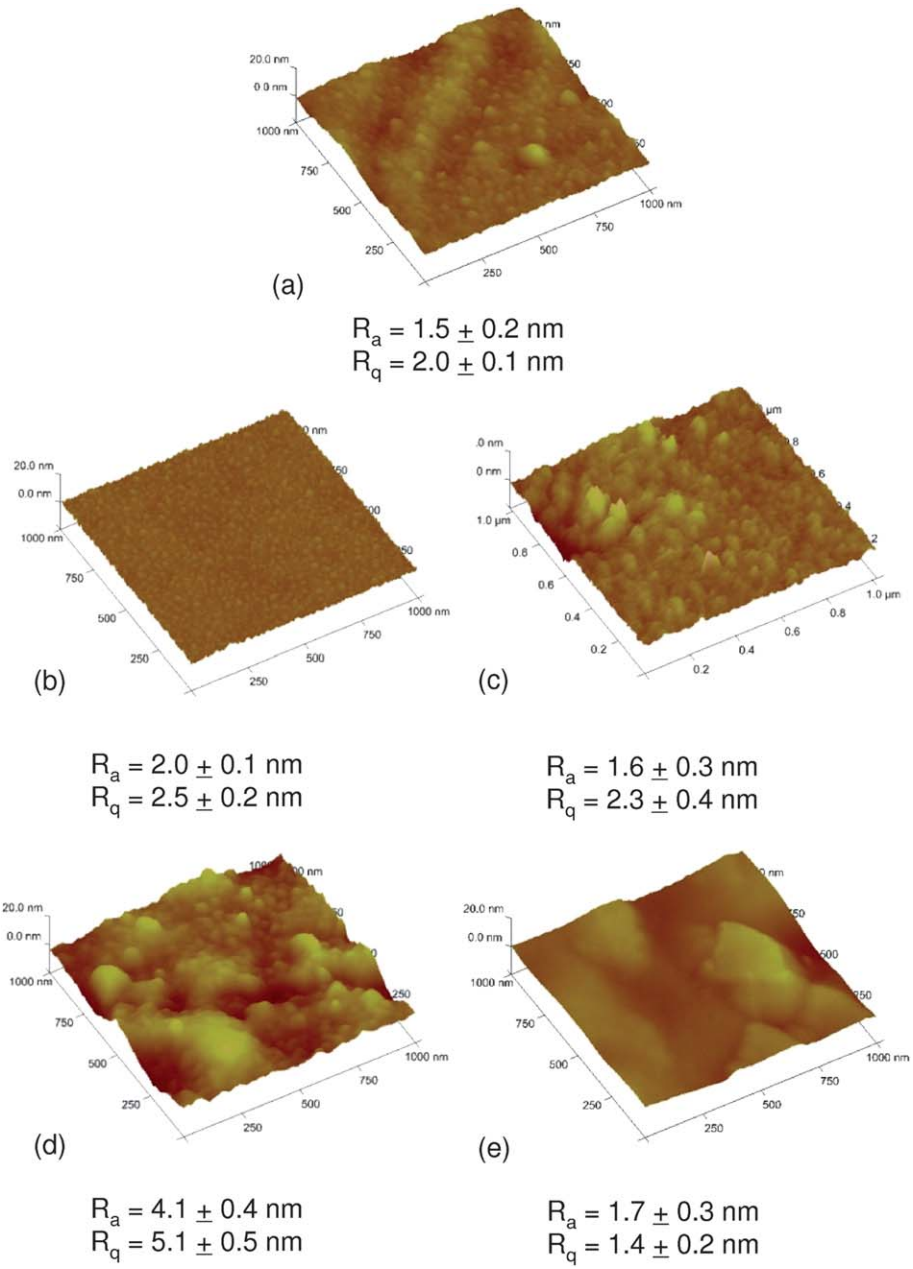

Fig. 5 AFM (1 μm × 1 μm) images for (a) pristine PS, (b) Psox, (c) PS-*g*-APTMS, (d) PS-*g*-HA_{1mg} and (e) PS-*g*-HA_{3mg}.

on the pristine PS surface appeared rounded and non-adherent and were completely washed away with a PBS rinse (Fig. 6a). Conversely, large numbers of LECs adhered to the PSox surface (Fig. 6b). Although washing of the surface with PBS resulted in removal of some of the more rounded cells, the majority appeared to be elongated and adherent. Staining with crystal violet further showed these cells to have a well spread morphology. Optical images of the LECs adhered onto the PS-*g*-APTMS layer showed that the cells in this case were less well spread in comparison to those on the PSox surface (Fig. 6c). There were a greater number of rounded cells on this surface which were subsequently washed away with PBS. Additional morphological evaluation of the cells *via* crystal violet staining showed them to be slightly shrunken, but still adherent. In general, it is known that cells adhere better to hydrophilic rather than hydrophilic surfaces.[38] Furthermore, it is also known that cells are sensitive to the chemistry and topography of materials.[38,57,58] Therefore, in the case of the PSox and PS-*g*-APTMS surface, the increase in cellular response is due to the hydrophilicity of the surface which due to the surface chemistry and topography.

The optical micrographs of the LECs on the PS-*g*-HA_{1mg} surface were rounded, although they were not all removed after PBS washing (Fig. 6d). Extremely poor cell adherence was obtained for the PS-*g*-HA_{3mg}, sample which corresponds to the surface most coherently grafted HA layer. This behaviour suggests that the HA in this latter sample exists in a conformation that allows it to act as a steric–entropic barrier. This surface condition is known to be cell-resistant due to the absence of proteins that provide cell anchorage to the surface. It was not possible to quantify the adhered cells on the PS-*g*-$HA_{1mg/3mg}$ samples by the colourimetric crystal violet assay due to the fact that HA absorbs the crystal violet dye.

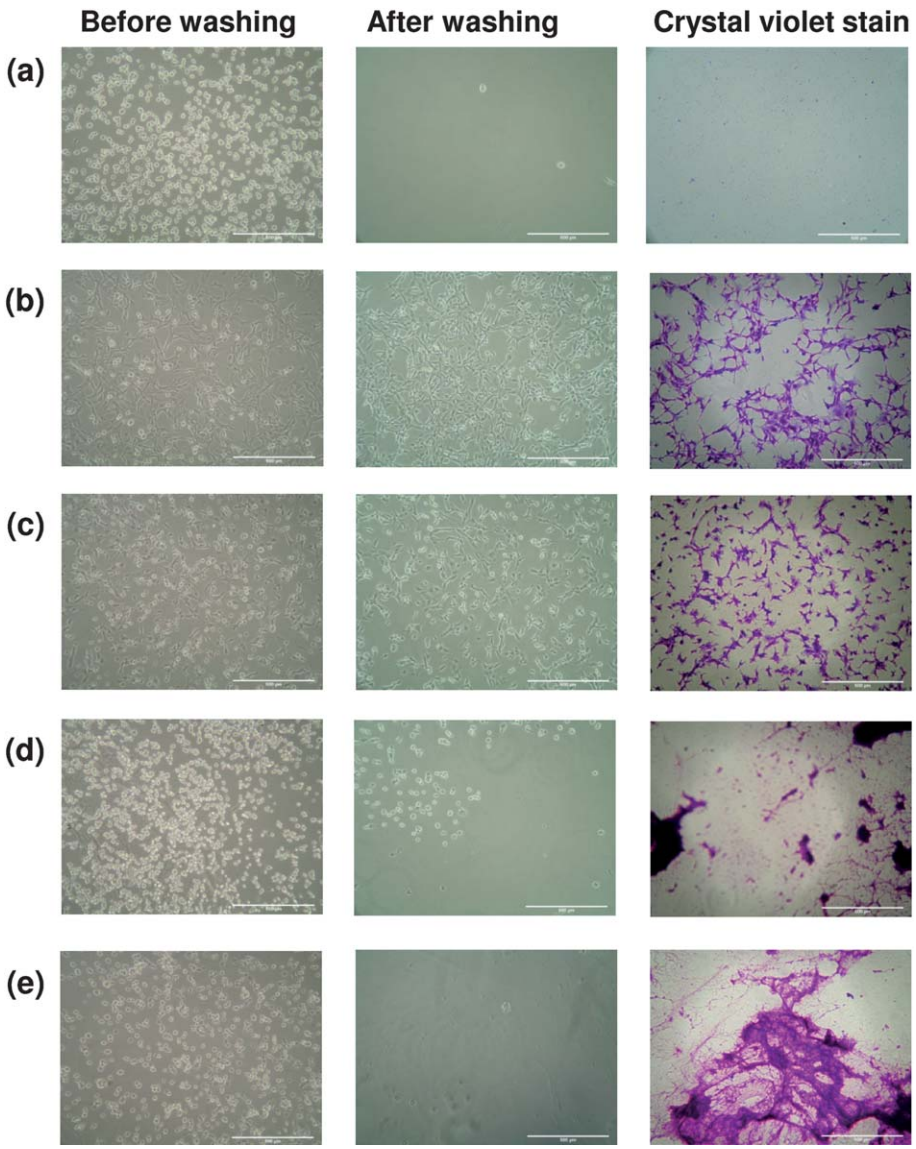

Fig. 6 Optical micrographs of LECs after 24 h in culture before washing, after washing and stained with crystal violet for (a) pristine PS, (b) Psox, (c) PS-*g*-APTMS, (d) PS-*g*-HA_{1mg} and (e) PS-*g*-HA_{3mg}. Scale bar represents 100 μm.

LEC viability on the various surfaces was further determined using the MTT assay with the data at 24 and 48 h post-seeding given in Fig. 7. Cell viability on PSox was found to be statistically higher ($p < 0.000005$) than that on both the pristine controls and the HA grafted surfaces (PS-*g*-HA_{1mg}, PS-*g*-HA_{3mg}). It is well known that cells need to attach and spread on a surface before they can undergo proliferation. Hence, these data reflect the cell adhesion assay results presented above. As such, it is clear that the LECs that have adhered onto the DBD treated PS surfaces after 4 hours in culture are viable and capable of proliferating, thereby indicating that this modified surface condition created, allows for an increased cellular response. The results also demonstrate that grafting of HA onto the PSox surface using a APTMS linker layer creates a condition that is highly resistant to cell adhesion and thereby proliferation for both the PS-*g*-HA_{1mg} and the PS-*g*-HA_{3mg} surfaces.

In order to further study the morphology of those LECs that adhered to the pristine and DBD-treated PS surfaces and to check the degree of resistance to cell adhesion offered by the HA grafted substrates, the cytoskeleton and nuclei of the cells in culture were fluorescently stained 24 h post-seeding. Fig. 8 shows representative fluorescent micrographs for each surface type. No cells were observed on the pristine polymer surface (Fig. 8a). By contrast, the cells on the DBD treated and APTMS functionalised PS had a well spread morphology with a high contact area (Fig. 8b and c). Similarly to the optical micrographs of the LECs on the PS-*g*-APTMS surface, the cells were shrunken in comparison to the PSox surface. This is the first time to the best of our knowledge that this type of aminated surface obtained by self assembly onto DBD treated surfaces, has been shown to enhance cellular response. As nitrogen functionalised surfaces are known to increase cellular response,[59] further studies on the long term cell viability of these aminated surfaces is being carried out and reported elsewhere. The cells on the PSox and PS-*g*-APTMS surface had produced actin stress fibres that formed a dense and complex network. These well spread morphologies are indicative of cells that are actively adhering and proliferating. A stable actin cytoskeletal structure for adherent cells is generally related to well formed attachments to the extracellular matrix (ECM)[60] and interactions with neighbouring cells.[61] Stress fibres

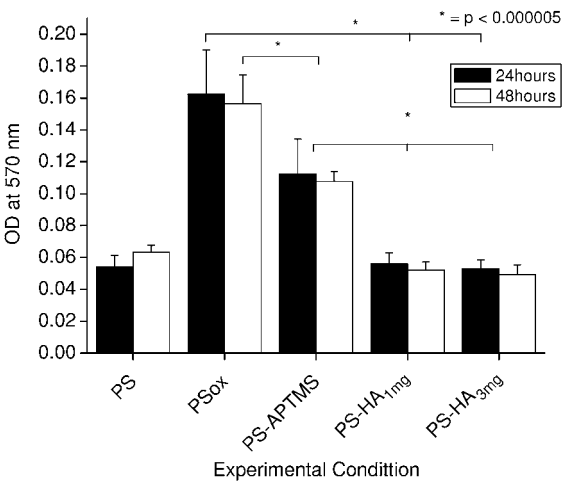

Fig. 7 MTT assay data for activity of LECs on the various PS samples 24 h and 48 h post-seeding.

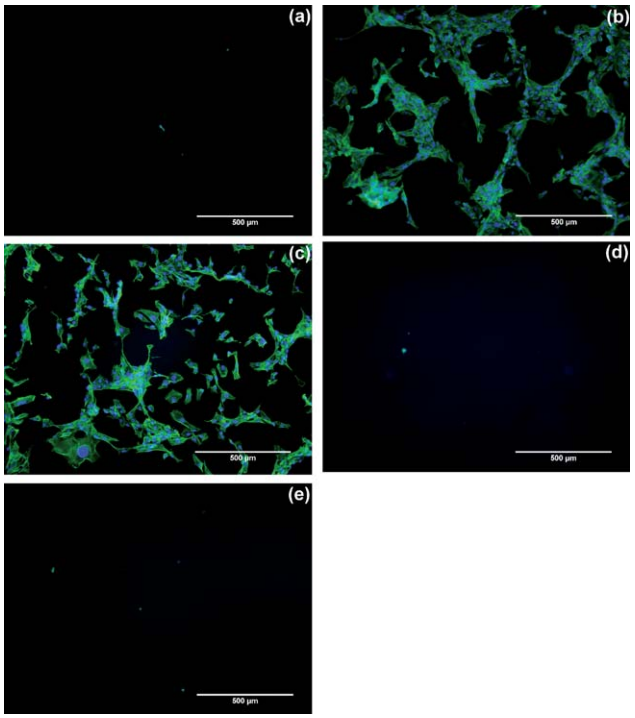

Fig. 8 Fluorescent micrographs of LECs dual stained with actin (green) and nuclei (blue) showing the cytoskeleton in cells 24 h post-seeding on (a) pristine PS, (b) Psox, (c) PS-*g*-APTMS, (d) PS-*g*-HA_{1mg} and (e) PS-*g*-HA_{3mg}. Scale bar represents 500 μm.

that are organised from actin filaments are associated with integrin receptors at the focal adhesion points where they control integrin signalling and integrin/matrix adhesion.[62–64] Again no cells were detected on the PS-*g*-HA_{1mg} and PS-*g*-HA_{3mg} surfaces under the experimental conditions used here (Fig. 8d and e). Since actin stress fibres are responsible for anchorage at the cell adhesion sites, it can be stated that adherence is substantially stronger on the DBD-treated and APTMS functionalised surfaces (with a well spread network of actin fibres) compared to pristine or HA-grafted surfaces (displaying no cells).

4 Conclusions

A method for immobilisation of hyaluronic acid (HA) on a polymer for the purposes of providing a surface condition that is resistant to adhesion of lens epithelial cells has been developed. The approach adopted uses atmospheric pressure dielectric barrier discharge plasma processing to enhance the chemisorption of 3-aminopropyltrimethoxysilane (APTMS) onto polystyrene (PS). Hyaluronic acid (HA) has then been successfully immobilised onto the aminosilane linker layer on PS *via* carbodiimide mediated chemical grafting. XPS analysis of the APTMS layer indicates the presence of three nitrogen species, namely: protonated amine, hydrogen-bonded amine and free amine. The availability of the nitrogen moiety is essential for the subsequent immobilisation of HA by carbodiimide coupling and the DBD treatment enhances their provision on the PS surface. The thickness of the grafted HA layers at the two concentrations employed (1 mg cm^{-3} and 3 mg cm^{-3}) were less than the XPS sampling depth in the "dry state". ToF-SIMS analysis indicated that each step was homogeneous on a 100 × 100 m^2 scale. Both

of these HA grafted surfaces were able to inhibit LEC attachment and growth. Although some cells were observed on the PS-*g*-HA_{1mg} surface, they were rounded and lacked the morphological characteristics indicative of attachment. The greatest level of resistance to cell adhesion was obtained for the PS-*g*-HA_{3mg}. This effect is attributed to the occurrence of a coherently grafted HA layer that is present in a conformation that allows it to act as a hydrated steric–entropic barrier, which confers cell-resistance due to the absence of attachment proteins that provide cell anchorage to the surface.

Acknowledgements

Financial Support from the Department for Employment and Learning, Northern Ireland under the Cross Border Research and Development Funding Programme – Strengthening the All-island Research Base for functional biomaterials (DE:-UU-05) is acknowledged.

References

1 D. G. Castner and B. D. Ratner, *Surf. Sci.*, 2002, **500**, 28–60.
2 B. Kasemo, *Surf. Sci.*, 2002, **500**, 656–677.
3 J. M. Anderson, *Annu. Rev. Mater. Res.*, 2001, **31**, 81–110.
4 J. M. Anderson, A. Rodriguez and D. T. Chang, *Semin. Immunol.*, 2008, **20**, 86–100.
5 M. Morra, *J. Biomater. Sci., Polym. Ed.*, 2000, **11**, 547–569.
6 P. Kingshott and H. J. Griesser, *Curr. Opin. Solid State Mater. Sci.*, 1999, **4**, 403–412.
7 R. A. D'Sa and B. J. Meenan, *Langmuir*, 2010, **26**, 1894–1903.
8 R. A. D'Sa, G. A. Burke and B. J. Meenan, *J. Mater. Sci.: Mater. Med.*, 2010, **21**, 1703–1712.
9 P. Kingshott, H. Thissen and H. J. Griesser, *Biomaterials*, 2002, **23**, 2043–2056.
10 R. Michel, S. Pasche, M. Textor and D. G. Castner, *Langmuir*, 2005, **21**, 12327–12332.
11 S. J. Sofia, V. Premnath and E. W. and Merrill, *Macromolecules*, 1998, **31**, 5059–5070.
12 H. Chen, Z. Zhang, Y. Chen, M. A. Brook and H. Sheardown, *Biomaterials*, 2005, **26**, 2391–2399.
13 S. L. McArthur, K. M. McLean, P. Kingshott, H. A. W. St John, R. C. Chatelier and H. J. Griesser, *Colloids Surf., B*, 2000, **17**, 37–48.
14 M. Van Beek, L. Jones and H. Sheardown, *Biomaterials*, 2008, **29**, 780–789.
15 M. Morra and C. Cassineli, *J. Biomater. Sci., Polym. Ed.*, 1999, **10**, 1107–1124.
16 M. Morra, *Biomacromolecules*, 2005, **6**, 1205–1223.
17 T. C. Laurent and J. R. E. Fraser, *Hyaluronan*, 1992, **6**, 2397–2404.
18 J. R. E. Fraser and T. C. Laurent, in *Extracellular Matrix, Volume 2: Molecular Components and Interactions*, ed. W. D. Comper, Harwood Academic Publishers, The Netherlands, 1996, pp. 141–199.
19 T. C. Laurent, in *Chemistry and Molecular Biology of the Intracellular Matrix*, ed. E. A. Balazas, Academic Press, London, 1970, pp. 703–732.
20 B. P. Toole, in *Cell Biology of Extracellular Matrix*, ed. E. D. Hay, Plenum Press, New York, 1991, p. 305.
21 T. Nishida, M. Nakamura, H. Mishima and T. Otori, *Exp. Eye Res.*, 1991, **53**, 753–758.
22 M. E. Johnson, P. J. Murphy and M. Boulton, *Graefe's Arch. Clin. Exp. Ophthalmol.*, 2006, **244**, 109–112.
23 M. B. Limberg, C. McCaa, G. E. Kissling and H. E. Kaufman, *Am. J. Ophthalmol.*, 1987, **103**, 194–197.
24 S. Suri and R. Banerjee, *J. Biomed. Mater. Res., Part A*, 2006, **79**, 650–664.
25 R. A. Stile, T. A. Barber, D. G. Castner and K. E. Healy, *J. Biomed. Mater. Res.*, 2002, **61**, 391–398.
26 L. Cen, K. G. Neoh and E. T. Kang, *Langmuir*, 2002, **18**, 8633–8640.
27 G. Chen, Y. Ito, Y. Imanishi, A. Magnani, S. Lamponi and R. Barbucci, *Bioconjugate Chem.*, 1997, **8**, 730–734.
28 M. Mason, K. P. Vercruysse, K. R. Kirker, R. Frisch, D. M. Marecak, G. D. Prestwich and W. G. Pitt, *Biomaterials*, 2000, **21**, 31–36.
29 Y. Park, N. Tirelli and J. A. Hubbell, *Biomaterials*, 2003, **24**, 893.
30 K. Y. Suh, J. M. Yang, A. Khademhosseini, D. Berry, T. N. Tran, H. Park and R. Langer, *J. Biomed. Mater. Res., Part B*, 2005, **72**, 292–298.
31 K. S. Siow, L. Britcher, S. Kumar and H. J. Griesser, *Plasma Processes Polym.*, 2006, **3**, 392–418.
32 J. M. Goddard and J. H. Hotchkiss, *Prog. Polym. Sci.*, 2007, **32**, 698–725.
33 B. Zhao and W. J. Brittain, *Prog. Polym. Sci.*, 2000, **25**, 677–710.
34 K. Kato, E. Uchida, E. T. Kang, Y. Uyama and Y. Ikada, *Prog. Polym. Sci.*, 2003, **28**, 209–259.
35 G. Borcia, C. A. Anderson and N. M. D. Brown, *Appl. Surf. Sci.*, 2004, **225**, 186–197.
36 G. Borcia, C. A. Anderson and N. M. D. Brown, *Appl. Surf. Sci.*, 2004, **221**, 203–214.
37 C. Z. Liu, J. Q. Wu, L. Q. Ren, J. Tong, J. Q. Li, N. Cui, N. M. D. Brown and B. J. Meenan, *Mater. Chem. Phys.*, 2004, **85**, 340–346.
38 R. A. D'Sa, G. A. Burke and B. J. Meenan, *Acta Biomater.*, 2010, **6**, 2609–2620.
39 C. Liu, N. M. D. Brown and B. J. Meenan, *Appl. Surf. Sci.*, 2006, **252**, 2297–2310.
40 C. Liu, N. Cui, N. M. D. Brown and B. J. Meenan, *Surf. Coat. Technol.*, 2004, **185**, 311–320.
41 N. Y. Cui, D. J. Upadhyay, C. A. Anderson, B. J. Meenan and N. M. D. Brown, *Appl. Surf. Sci.*, 2007, **253**, 3865–3871.
42 D. J. Upadhyay, N. Y. Cui, B. J. Meenan and N. M. D. Brown, *J. Phys. D: Appl. Phys.*, 2005, **38**, 922–929.
43 J. Chastain, *Handbook of X-Ray Photoelectron Spectroscopy*, Perkin-Elmer Corporation, Minnesota, 1992.
44 R. G. Thomas, R. V. Zoran, C. C. Ronald and J. G. Hans, *J. Polym. Sci., Part A: Polym. Chem.*, 1994, **32**, 1399–1414.
45 P. Kingshott, S. McArthur, H. Thissen, D. G. Castner and H. J. Griesser, *Biomaterials*, 2002, **23**, 4775–4785.
46 L. Zhang, Y. Chen and T. Dong, *Surf. Interface Anal.*, 2004, **36**, 311–316.
47 G. C. Allen, F. Sorbello, C. Altavilla, A. Castorina and E. Ciliberto, *Thin Solid Films*, 2005, **483**, 306–311.
48 K. Bierbaum, M. Kinzler, C. Woell, M. Grunze, G. Haehner, S. Heid and F. Effenberger, *Langmuir*, 1995, **11**, 512–518.
49 P. Harder, K. Bierbaum, C. Woell, M. Grunze, S. Heid and F. Effenberger, *Langmuir*, 1997, **13**, 445–454.
50 J. L. Magalhães, L. M. Moreira, U. P. Rodrigues-Filho, M. J. Giz, M. A. Pereira-da-Silva, R. Landers, R. C. G. Vinhas and P. A. P. Nascente, *Surf. Interface Anal.*, 2002, **33**, 293–298.
51 J. H. Moon, J. H. Kim, K. j. Kim, T. H. Kang, B. Kim, C. H. Kim, J. H. Hahn and J. W. Park, *Langmuir*, 1997, **13**, 4305–4310.
52 Z. Q. Wei, C. Wang, C. F. Zhu, C. Q. Zhou, B. Xu and C. L. Bai, *Surf. Sci.*, 2000, **459**, 401–412.
53 E. M. E. Kristensen, F. Nederberg, H. Rensmo, T. Bowden, J. Hilborn and H. Siegbahn, *Langmuir*, 2006, **22**, 9651–9657.
54 D. Kowalczyk, S. Slomkowski, M. M. Chehimi and M. Delamar, *Int. J. Adhes. Adhes.*, 1996, **16**, 227–232.
55 T. J. Horr and P. S. Arora, *Colloids Surf., A*, 1997, **126**, 113–121.
56 C. H. Chiang, H. Ishida and J. L. Koenig, *J. Colloid Interface Sci.*, 1980, **74**, 396–404.
57 M. S. Lord, M. Foss and F. Besenbacher, *Nano Today*, 2010, **5**, 66–78.
58 K. Anselme, L. Ploux and A. Ponche, *J. Adhes. Sci. Technol.*, 2010, **24**, 831–852.
59 L. C. Lopez, M. R. Belviso, R. Gristina, M. Nardulli, R. d'Agostino and P. Favia, *Plasma Processes Polym.*, 2007, **4**, S402–S405.
60 S. Wiesner, K. R. Legate and R. Fassler, *Cell. Mol. Life Sci.*, 2005, **62**, 1081–1099.
61 B. Angres, A. Barth and W. J. Nelson, *J. Cell Biol.*, 1996, **134**, 549–557.
62 S. Miyamoto, H. Teramoto, O. A. Coso, J. S. Gutkind, P. D. Burbelo, S. K. Akiyama and K. M. Yamada, *J. Cell Biol.*, 1995, **131**, 791–805.
63 Y. Nojima, N. Morino, T. Mimura, K. Hamasaki, H. Furuya, R. Sakai, T. Sato, K. Tachibana, C. Morimoto, Y. Yazaki and H. Hirai, *J. Biol. Chem.*, 1995, **270**, 15398–15402.
64 S. J. Shattil, B. Haimovich, M. Cunningham, L. Lipfert, J. T. Parsons, M. H. Ginsberg and J. S. Brugge, *J. Biol. Chem.*, 1994, **269**, 14738–14745.